Journal of Zhejiang University-SCIENCE A (Applied Physics & Engineering) 2023 24(11):978-990
www.jzus.zju.edu.cn; www.springer.com/journal/11582
E-mail: jzus_a@zju.edu.cn

Research Article

https://doi.org/10.1631/jzus.A2200430

Experimental investigation on cenosphere-aluminum syntactic foam-filled tubes under axial impact loading

Li WANG[1,2], Boyi ZHANG[1,2]✉, Jian ZHANG[1,2], Yuexin JIANG[1,2], Wei WANG[1,2], Gaohui WU[3]

[1]*School of Civil Engineering, Harbin Institute of Technology, Harbin 150090, China*
[2]*Key Lab of Structures Dynamic Behavior and Control of the Ministry of Education, Harbin Institute of Technology, Harbin 150090, China*
[3]*Center for Metal Matrix Composites Engineering Technology, Harbin Institute of Technology, Harbin 150006, China*

Abstract: A new syntactic foam material was prepared by screening three different average particle sizes of cenospheres (150, 200, and 300 μm) from industrial waste fly ash. Axial impact testing on syntactic foam filler and foam-filled tubes was conducted using a drop hammer test machine. The effects of parameters, such as the size of cenospheres and the impact velocity, on the mechanism of deformation, mechanical characteristics, and capacity for energy absorption of the specimen were investigated. On this basis, the differences in compressive properties exhibited by the syntactic foam-filled tubes under the two loading conditions were investigated. The results indicate that with the decrease in the average diameter of cenospheres, the initial peak crushing load and mean crushing load of foam-filled tubes increase, while the compression efficiency decreases. The specific energy absorption (SEA) of the syntactic foam-filled tube can reach 25 J/g. With the increase of impact velocity, the SEA of the specimen increases slightly. It was demonstrated that the syntactic foam-filled tube exhibits a higher effective energy absorption ratio under impact loading compared to quasi-static loading.

Key words: Cenosphere-aluminum syntactic foam; Crashworthiness; Mechanical properties; Absorption of energy

1 Introduction

Over the past decades, in the face of frequent traffic accidents, there has been much research on energy-absorbing components to prevent personal injuries. Thin-walled tubes have attracted extensive attention because of their convenient preparation and good energy absorption capacity (Xu et al., 2017; Zou et al., 2017; Sun et al., 2018; Ferdynus et al., 2019; Mansor et al., 2022; Zha et al., 2022). Significant research has been undertaken on the crushing behavior of thin-walled tubes with various cross-sections, including triangular tubes, round tubes, square tubes, and corrugated tubes (Wu et al., 2016; Zhang et al., 2018; Wang et al., 2019; Sadsighi et al., 2022; Ghahremanzadeh and Pirmohammad, 2023).

To further improve the characteristics of components for energy absorption, metallic foams (Sun et al., 2016; Liu ZF et al., 2017; Zhang et al., 2021) and polymeric foams (Yan et al., 2014; Hussein et al., 2017; Liu Q et al., 2017; Sarkabiri et al., 2017; Ghamarian and Azarakhsh, 2019) are usually inserted in thin-walled tubes as fillers. Djamaluddin et al. (2015) used non-dominated sorting genetic algorithm (NSGA-II) to optimize the design of the crashing behavior of an empty double-tube, a foam-filled empty tube, and a foam-filled double-tube under axial and oblique impact loadings. Results showed that the crashworthiness of the foam-filled double-tube was about 12% better than that of the others. Hu et al. (2018) presented an aluminum foam-filled tri-tube and noted that the outer tube's diameter and wall thickness had a strong impact on the energy absorption capacity of specimens. The research by Hu et al. (2018) showed that for the aluminum foam-filled tri-tube, the influence of the outer tube's wall thickness on the energy absorption performance of the specimen was very obvious. Abedi et al. (2018) investigated polyurethane foam-filled grooved tubes with circular cross-sections. The results showed that when the groove distance is large, the manner of deformation of the foam-filled tube tends to be the diamond

✉ Boyi ZHANG, zhangby@hit.edu.cn
Boyi ZHANG, https://orcid.org/0000-0002-6443-8154

Received Sept. 15, 2022; Revision accepted Jan. 21, 2023;
Crosschecked July 22, 2023; Online first Sept. 8, 2023

mode, and when the groove distance is small, the deformation mode tends to be the concertina mode. Movahedi and Linul (2017, 2021), Linul et al. (2018), and Movahedi et al. (2018) conducted much experimental research on the compression behavior of aluminum alloy foam-filled tubes at elevated temperatures. The effect of temperature on the mechanical properties of foam-filled tubes was explored in depth. Mohammadiha and Ghariblu (2018) studied the axial dynamic energy absorption properties of a foam-filled free inversion tube. According to deformation theory, they derived analytical formulas for the instantaneous reversal load of a foam-filled tube during free inversion by applying a new theoretical model. Duarte et al. (2018) analyzed the mechanical performance of extremely thin-walled aluminum alloy in-situ foam-filled tubes and pointed out that during the preparation process, the thermal treatment of the thin-walled tubes can enhance their ductility and reduce the probability of crack formation.

Compared with traditional foam-filled tubes, the crashworthiness of syntactic foam-filled tubes needs further study. Several scholars have carried out research on the influences of the syntactic foam preparation method (Kemény et al., 2022) and loading direction (Su et al., 2019) on the compressive properties of foam-filled tubes. Movahedi et al. (2022) further discussed the deformation mode of functionally graded metal syntactic foams under high-speed impact loading. Fly ash cenosphere is a kind of common industrial waste, which is gradually being used in the preparation of composite materials (Mondal et al., 2009; Braszczyńska-Malik et al., 2017). The cenosphere-aluminum syntactic foam not only has excellent energy absorption capacity, but also has a certain bearing capacity (Doddamani et al., 2015; Manakari et al., 2016; Zhang et al., 2016; Garcia et al., 2018). Combining this material with metal tubes to prepare foam-filled tube specimens can both reduce environmental pollution and reduce the preparation cost of composite foam, and will have broad application potential.

The crushing behavior of cenosphere-aluminum syntactic foam under an axial quasi-static load has been studied (Wang et al., 2021). This paper investigates the mechanical properties of syntactic foam-filled tubes under axial low-velocity impact loading. The effects of impact load velocity and the average particle size of cenospheres on the energy absorption capacity of the specimens are analyzed. The differences in deformation modes and energy absorption ratios of syntactic foam-filled tubes under different loading conditions are indicated. The organization of this paper is as follows. Section 2 introduces the preparation of the syntactic foam, the geometric parameters of specimens, and the loading scheme of the test. The evaluation indexes of the specimen under impact loading, such as initial peak crushing load, mean crushing load, and specific energy absorption (SEA), are analyzed in Section 3. Section 4 compares the foam-filled tube's crashworthiness under impact and quasi-static loads, and conclusions are presented in Section 5.

2 Materials

2.1 Material and specimen

Pressure infiltration was employed to create the cenosphere-aluminum syntactic foam used in this test. There are three types of cenospheres (58.8% SiO_2, 26.1% Al_2O_3) (mass fraction), with typical particle sizes of 150, 200, and 300 μm, which were obtained by screening industrial fly ash. Then, the molten 1199Al (0.005% Cu, 0.003% Fe, and 0.0025% Si (mass fraction) balanced with Al as the main alloying element) was injected into the mold with cenosphere preforms, and gradually pressurized so that the voids of preforms were filled with liquid aluminum. The preparation method of the material is shown in Fig. 1.

The thin-walled empty tube used in the experiment is 6063 aluminum alloy seamless tube with outer diameter of 20 mm, wall thickness of 1.2 mm, and height of 30 mm. The material properties of 6063 aluminum alloy (0.51% Si, 0.64% Mg, and 0.27% Fe balanced with Al as the main alloying element) were obtained through uniaxial tension test, as shown in Fig. 2a. The stress–strain (σ-ε) curve of 6063 aluminum alloy shows four main stages: elastic stage, yield stage, strain-hardening stage, and fracture stage. Cenosphere-aluminum syntactic foam is used as the filler, and each type of cenosphere has an average particle size of 150, 200, and 300 μm. The stress–strain curves of the three types of cenosphere-aluminum syntactic foam (150SF, 200SF, and 300SF) are shown in Fig. 2b. The stress–strain curve of syntactic foam shows typical three-stage characteristics: linear elastic stage, plastic plateau stage, and compression densification stage (Duarte et al., 2018).

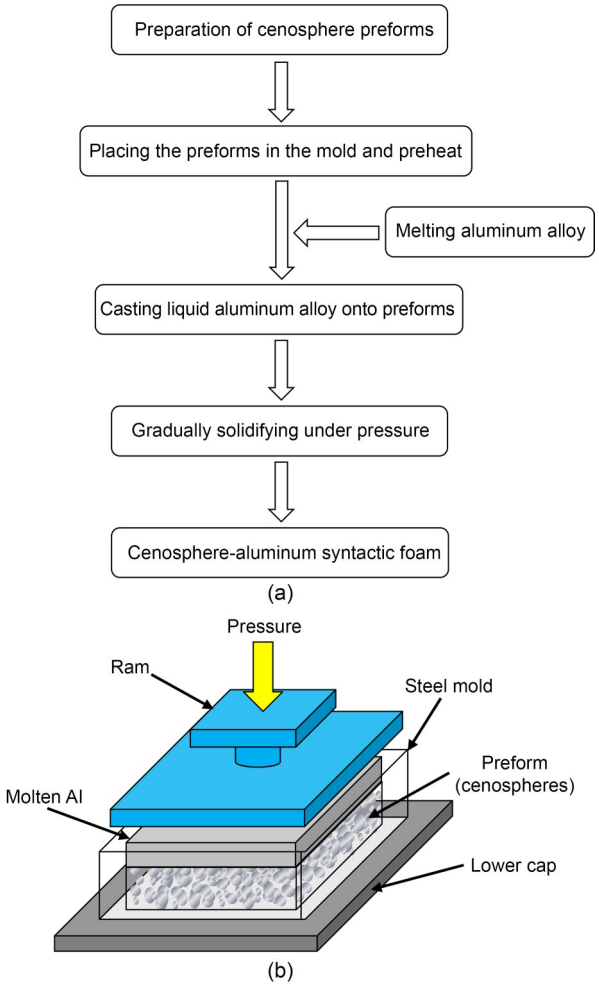

Fig. 1 Preparation method of cenosphere-aluminum syntactic foam: (a) preparation flow chart; (b) preparation process diagram

The syntactic foam specimens used in the experiment are shown in Fig. 3. Fig. 4 is the diameter distribution of cenospheres. The microstructure of syntactic foam is shown in Fig. 5. In the figure, bright areas are the aluminum matrix, and dark areas are cenospheres, which maintain a complete appearance and are spread equally throughout the aluminum matrix. The geometries and dimensions of specimens are listed in Table 1. In the specimen number, AX indicates axial impact, and T1.2 indicates that the tube wall thickness is 1.2 mm. The numbers 150, 200, and 300 indicate the different types of cenosphere-aluminum syntactic foam with varying average particle sizes. The numbers 5 and 6 represent the impact velocities of 5 and 6 m/s. AX-150-6, AX-200-6, and AX-300-6 respectively represent different syntactic foam cylinder specimens, and the others are foam-filled tubes.

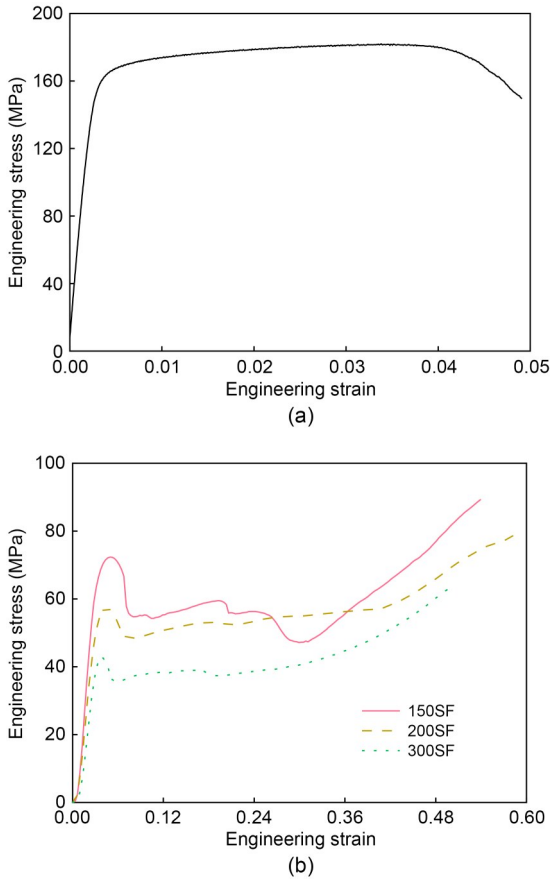

Fig. 2 σ-ε curves of material: (a) aluminum alloy; (b) syntactic foam

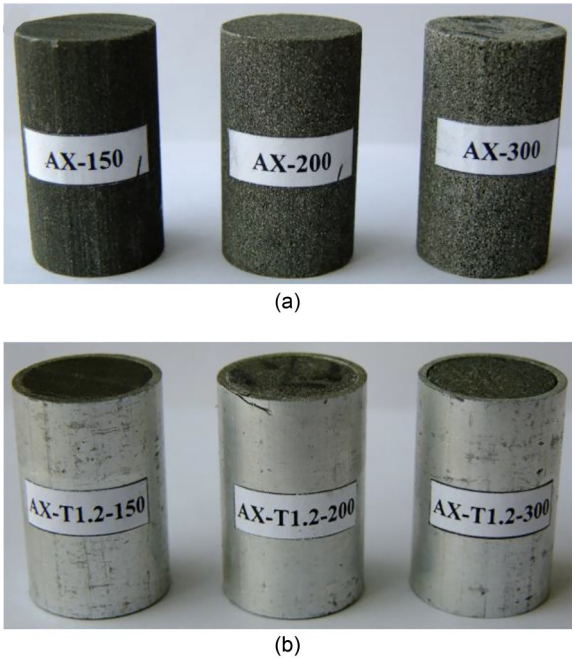

Fig. 3 Specimens used in impact test: (a) syntactic foam filler; (b) syntactic foam-filled tubes

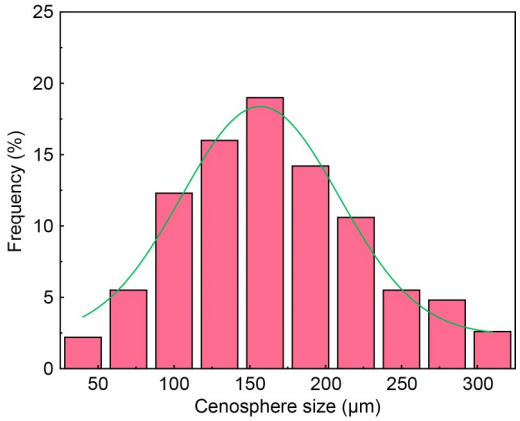

Fig. 4 Diameter distribution of cenospheres

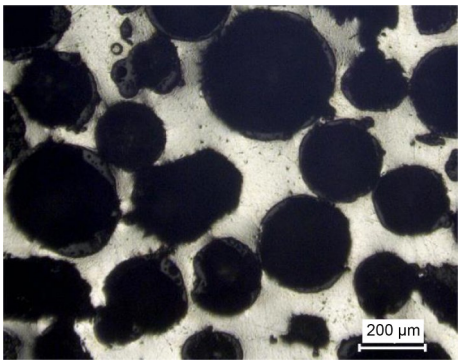

Fig. 5 Microstructure of syntactic foam

2.2 Experimental scheme

The axial impact experiment was conducted on the INSTRON 9250HV drop hammer test machine. The experimental set-up is shown in Fig. 6. The maximum drop height of the drop hammer is 4 m. The upper part of the testing machine is additionally provided with a spring, which can increase the initial speed of the drop hammer. The maximum impact speed of the drop hammer can reach 10 m/s. Through the built-in optical acquisition system, the test machine can obtain the displacement of the drop hammer during the entire impact process. At the same time, the acceleration sensor installed on the indenter can collect the acceleration of the drop hammer. The testing machine can be controlled in two ways: impact speed and impact energy. After determining the weight of the drop hammer, the system will automatically adjust the height of the drop hammer and the compression length of the spring. The relationship between the impact speed of the drop hammer and the initial potential energy is as follows:

$$v_t = \sqrt{\frac{2\left(mgh + \frac{1}{2}k(\Delta l)^2\right)}{m}}, \tag{1}$$

where v_t is the impact speed, h is the initial height of the drop hammer, m is the weight of the drop hammer, Δl and k are the compression and elastic modulus of the spring, respectively, and g is the acceleration under gravity.

Fig. 6 Experimental set-up

In this experiment, the impact mass is 22.71 kg. The impact velocities are 5 and 6 m/s. Specific parameters are shown in Table 1.

3 Impact experiment results

3.1 Failure mode

3.1.1 Syntactic foam filler

Fig. 7 illustrates the final shape of three syntactic foam fillers. Under the impact loading with a velocity of 6 m/s, the three kinds of filler were completely collapsed and expanded radially in a crushed shape.

3.1.2 Syntactic foam-filled tubes

The foam-filled tubes also show concertina failure mode under impact loading, as shown in Fig. 8. Compared with the cenosphere-aluminum syntactic foam bearing the impact load alone, due to the restraining

Table 1 Geometric parameters of specimens

Specimen No.	Outside diameter (mm)	Wall thickness (mm)	Average diameter of cenosphere (μm)	Height (mm)	Impact velocity (m/s)	Drop mass (kg)
AX-150-6	–	–	150	30	6	22.71
AX-200-6	–	–	200	30	6	22.71
AX-300-6	–	–	300	30	6	22.71
AX-T1.2-150-5	20	1.2	150	30	5	22.71
AX-T1.2-200-5	20	1.2	200	30	5	22.71
AX-T1.2-300-5	20	1.2	300	30	5	22.71
AX-T1.2-150-6	20	1.2	150	30	6	22.71
AX-T1.2-200-6	20	1.2	200	30	6	22.71
AX-T1.2-300-6	20	1.2	300	30	6	22.71

Fig. 7 Specimens after impact loading: (a) AX-150-6; (b) AX-200-6; (c) AX-300-6

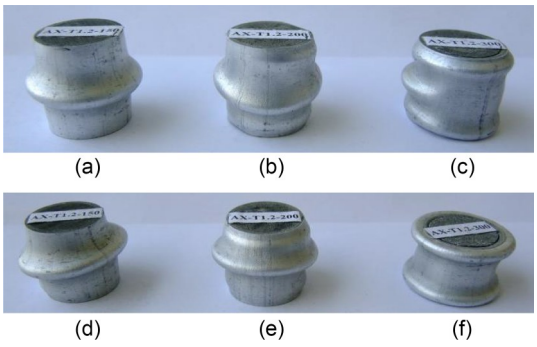

Fig. 8 Specimens after impact loading: (a) AX-T1.2-150-5; (b) AX-T1.2-200-5; (c) AX-T1.2-300-5; (d) AX-T1.2-150-6; (e) AX-T1.2-200-6; (f) AX-T1.2-300-6

effect of the aluminum tube on the filler, the foam-filled tubes maintain their integrity without collapse. With the increase of impact velocity, the axial deformation of the specimen increases obviously, but the failure mode basically does not change. It is noteworthy that specimen AX-T1.2-300-5 exhibits different deformation mechanisms under impact loading. This may be due to errors in the preparation and processing of the syntactic foam, which makes the specimen have certain initial defects. Under the impact load, the folds are concentrated on one side of the specimen.

Fig. 9 is a comparison between the final shape of specimen AX-T1.2-150-6 (Fig. 9a) and specimen AX-T1.2-300-6 (Fig. 9b). It was found that at the same

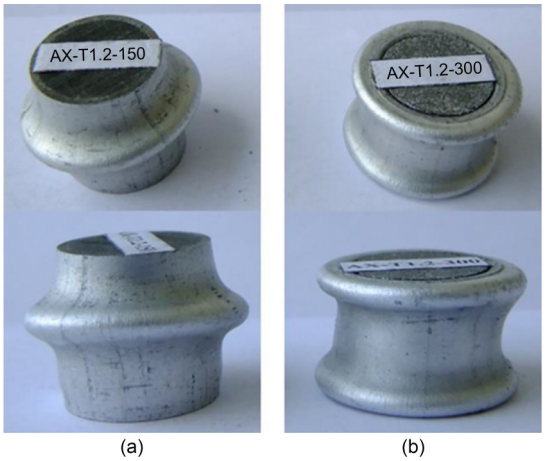

Fig. 9 Comparison between the final shapes of specimens: (a) AX-T1.2-150-6; (b) AX-T1.2-300-6

impact velocity, the axial distortion of the foam-filled tube increases with the increase of the average particle size of cenospheres in the filler. The specimen AX-T1.2-150-6 only forms a fold in the middle, while the specimen AX-T1.2-300-6 forms a fold at the upper and lower ends. This is because part of the filler in the specimen AX-T1.2-150-6 is broken under the impact load, so that the deformation is concentrated in the middle part of the foam-filled tube. This indicates that the porosity of the syntactic foam rises as the diameter of the cenospheres in the filler grows, increasing the compression deformation capacity of the foam-filled tube.

3.2 Dynamic mechanical properties

3.2.1 Load-displacement curves

The load-displacement curves of each set of specimens acquired in the experiment are shown in Fig. 10. Three kinds of syntactic foam filler exhibit typical

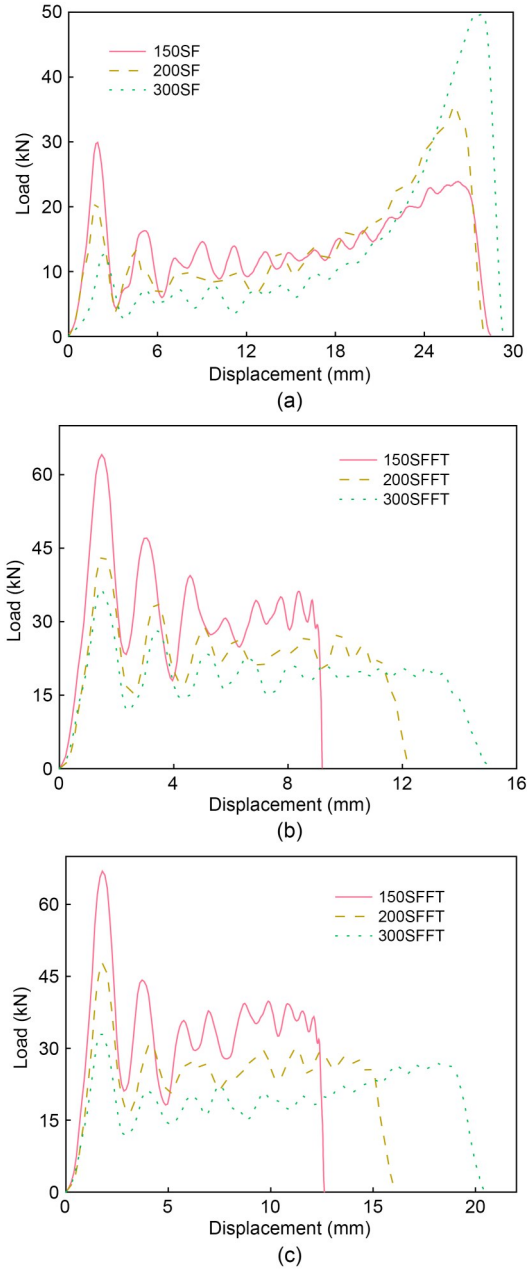

Fig. 10 Load-displacement curves of specimens: (a) AX-6; (b) AX-T1.2-5; (c) AX-T1.2-6

three-stage features of elastic stage, plastic plateau stage, and densification stage under impact load (Fig. 10a). This may be because the impact resistance of the specimen is distinctly improved by the aluminum tube, so that the impact load fails to compress the specimen to the densification stage. Compared with the peak load, the load of three types of syntactic foam in the plateau stage is relatively close. In the densification stage, the load of 300SF far exceeds the load of the other two kinds of syntactic foam. This is because the porosity of 300SF is the largest and the specimen becomes the densest under the impact load.

The characteristics of load–displacement curves of syntactic foam-filled tubes (150SFFT, 200SFFT, 300SFFT) under two kinds of impact velocities are basically the same, but there is no densification stage in the curves (Figs. 10b and 10c). Unlike the syntactic foam that bears the impact load alone, the foam-filled tubes show obvious strength differences during the plateau stage. Of the different types of foam-filled tubes, the compression stroke of 300SFFT is the largest, while the compression stroke of 150SFFT is the smallest.

In this study, a set of parameters are proposed and compared to assess the crashworthiness of energy-absorbing materials and components under impact load (Hanssen et al., 2000; Hou et al., 2007; Guler et al., 2010; Sun et al., 2010). The relevant experimental parameters for all specimens are summarized in Table 2. The following is the definition of the energy absorption efficiency f (Hanssen et al., 2000):

$$f=\frac{\int_0^s F(s)\mathrm{d}s}{F_{\max}H}, \tag{2}$$

where $F(s)$ is the impact loading, s is the compression stroke, $F_{\max}$ is the maximum impact loading in the range [0, s], and H is the height of the specimen. As the compression stroke lengthens, so does the energy absorption efficiency. The effective compression stroke S_{ef} is defined as the corresponding compression stroke when the energy absorption efficiency achieves its greatest value (Fig. 11). In the case of some load–displacement curves with no densification tendency, the effective compression stroke is taken as the entire compression stroke.

3.2.2 Peak crushing loading

The peak crushing loading F_{p} of foam-filled tubes and syntactic foam under axial impact loading is presented in Fig. 12. The figure shows that the peak crushing loading of 150SFFT is the highest, and the peak crushing loadings of 200SFFT and 300SFFT decrease sequentially. The aluminum tube restricts the cracking and radial expansion of the filler, which enhances the peak crushing loading of the foam-filled tube.

Table 2 Mechanical properties of the syntactic foam specimens

Specimen type	Peak crushing loading, F_p (kN)	Mean crushing loading, F_m (kN)	CLE	Effective energy absorption, W_{ef} (J)	SEA (J/g)
AX-150-6	30.0	12.5	41.7	276.8	18.9
AX-200-6	20.7	11.0	53.4	239.9	15.3
AX-300-6	12.6	6.8	54.0	136.6	9.8
AX-T1.2-150-5	64.2	31.8	49.5	282.9	17.4
AX-T1.2-200-5	43.6	22.5	51.7	277.0	15.8
AX-T1.2-300-5	36.6	18.3	50.0	276.1	16.6
AX-T1.2-150-6	66.9	33.3	49.8	407.8	25.1
AX-T1.2-200-6	47.6	24.2	50.9	394.9	22.0
AX-T1.2-300-6	33.0	19.4	58.8	398.9	23.9

CLE: crushing load efficiency

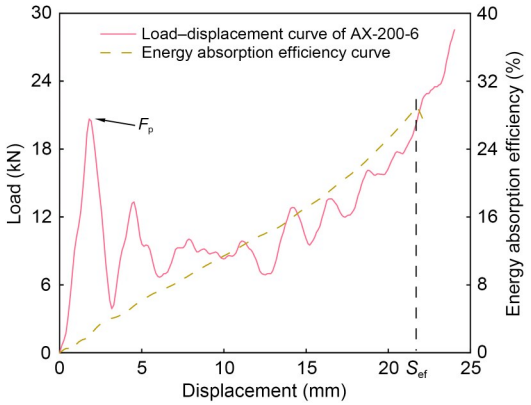

Fig. 11 Energy absorption efficiency curve and load–displacement curve

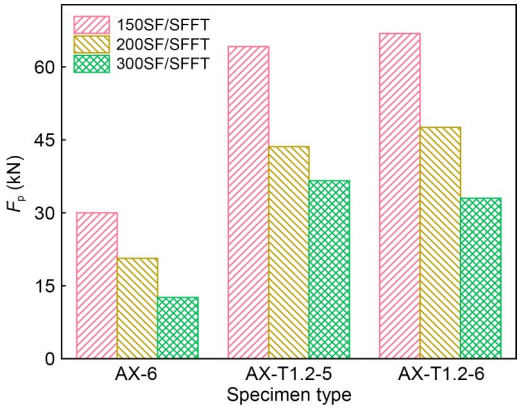

Fig. 12 Peak crushing loading of specimens

3.2.3 Mean crushing loading

The mean crushing loading F_m primarily represents the specimen's load level during the energy absorption process, which is described as (Sun et al., 2010):

$$F_m = \frac{\int_0^{S_{ef}} F(s)\mathrm{d}s}{S_{ef}}. \tag{3}$$

The mean crushing loading of syntactic foam and foam-filled tubes under axial impact load is shown in Fig. 13. The variation trend of the mean crushing loading of specimens is basically consistent with that of the initial peak crushing load. However, the mean crushing loads of three kinds of syntactic foam filler are closer, among which the mean crushing load of 150SF is only 13.6% higher than that of 200SF. The restraining effect of the aluminum tube on the syntactic foam filler can significantly increase the mean crushing loading of the specimen. The mean crushing loading of the foam-filled tube is enhanced by 156% on average when compared to the syntactic foam filler. The increase in impact velocity has little effect on the mean crushing loading of the specimen.

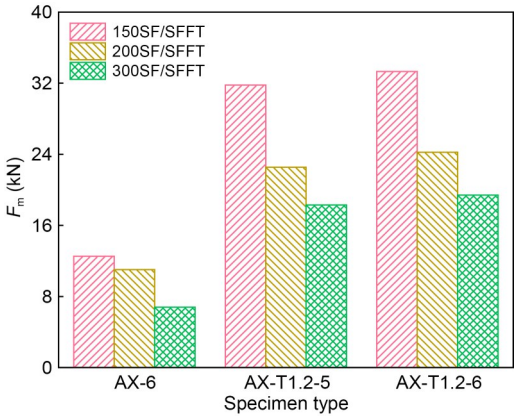

Fig. 13 Mean crushing loading of specimens

3.2.4 Crushing load efficiency (CLE)

The ideal energy-absorbing structure can not only fully absorb the impact energy, but also ensure the stability of the bearing capacity. CLE is an evaluation index of load consistency under impact load, defined as (Hanssen et al., 2000):

$$\mathrm{CLE}=\frac{F_{\mathrm{m}}}{F_{\mathrm{p}}}\times 100\%. \tag{4}$$

Fig. 14 plots the CLE of each specimen. When the impact velocity is 5 m/s, the CLE of the three types of foam-filled tubes varies little. When the impact velocity is 6 m/s, it can be found that the syntactic foam and foam-filled tubes gradually increase in CLE as the particle size of the cenospheres increases, which means that the initial impact effect of the specimen decreases.

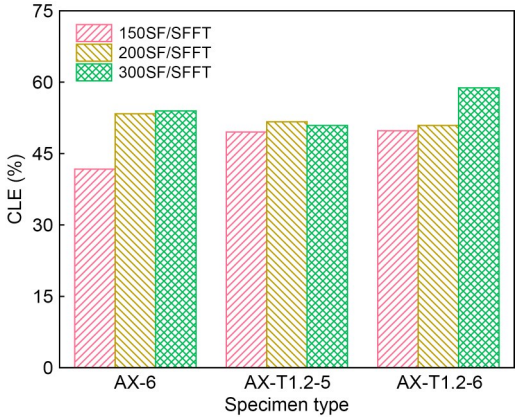

Fig. 14 CLE of specimens

3.3 Capacity for energy absorption

3.3.1 Effective energy absorption

The effective energy absorption W_{ef} mainly measures the energy absorption capacity of the sample in the plastic deformation stage. Its definition is as follows (Sun et al., 2010):

$$W_{\mathrm{ef}}=\int_0^{S_{\mathrm{ef}}}F(s)\mathrm{d}s. \tag{5}$$

Fig. 15 depicts the effective energy absorption of each sample. Combined with the experimental phenomena, it can be found that the aluminum tube can restrain the deformation of the syntactic foam filler to avoid being crushed and can greatly boost the specimen's effective energy absorption. Since none of the load–displacement curves of the foam-filled tubes reaches the densification stage, the effective energy absorption of the specimen is only related to the impact velocity. Under the same impact velocity, the difference in effective energy absorption of various foam-filled tubes is not obvious.

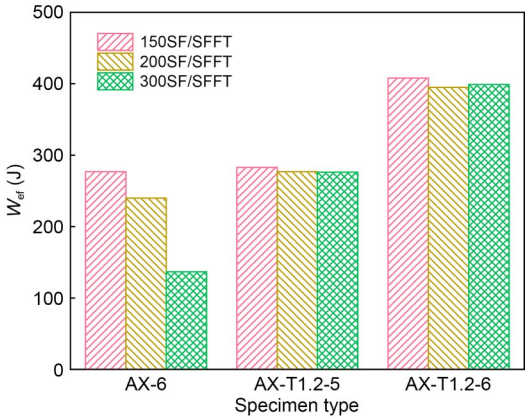

Fig. 15 Effective energy absorption of specimens

Fig. 16 compares the load–displacement superposition curve of the syntactic foam filler (AX-150-6) and the empty aluminum tube (ET) with the load–displacement curve of specimen AX-T1.2-150-6. The shaded area is the increment of effective energy absorption caused by the interaction effect. The percentage of effective energy absorption due to the interaction effect in each specimen is shown in Fig. 17. It can be found that the interaction effect between the syntactic foam filler and the aluminum tube is gradually enhanced with the decrease of the average particle size of cenospheres under the impact load.

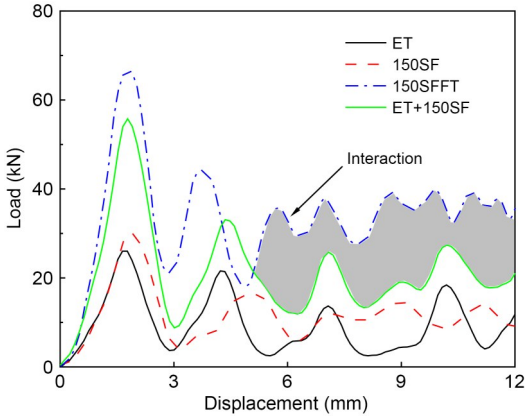

Fig. 16 Interaction effect of specimen AX-T1.2-150-6

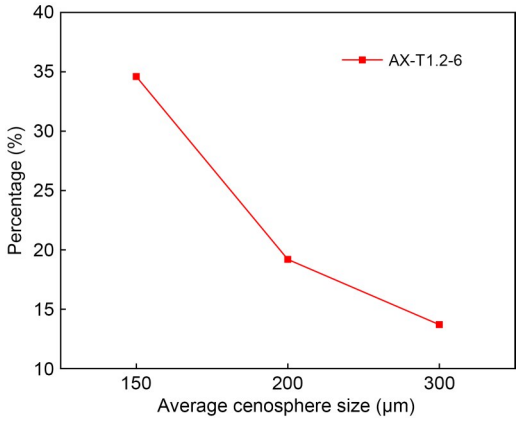

Fig. 17 Percentage of effective energy absorption due to the interaction effect

3.3.2 Specific energy absorption (SEA)

The SEA represents the amount of energy absorbed per unit mass of sample in the effective compression stroke, and is defined as follows (Sun et al., 2010):

$$\mathrm{SEA}=\frac{W_{\mathrm{ef}}}{\Delta m}=\frac{\int_0^{S_{\mathrm{ef}}}F(s)\mathrm{d}s}{\Delta m}, \tag{6}$$

where Δm is the mass of the specimen. The SEA of several types of specimens under impact loading is depicted in Fig. 18. The results indicate that, as the particle size in the filler increases, the SEA of the specimen decreases. Each syntactic foam-filled tube has an SEA of over 15 J/g, of which the SEA of 150SFFT reaches 25 J/g. As shown in Fig. 19, the syntactic foam-filled tube (specimen AX-T1.2-150-6) exhibited better energy absorption capacity under low-velocity impact loading compared to the polyurethane foam-filled tube

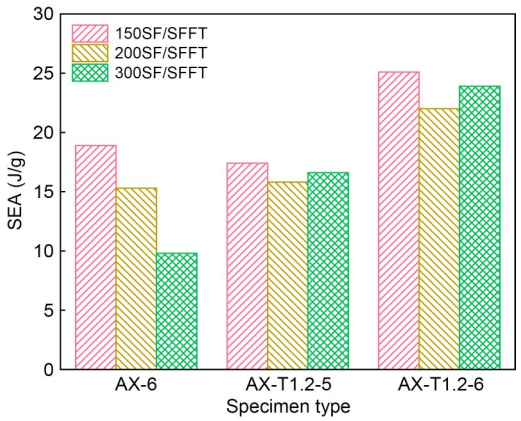

Fig. 18 SEA of specimens

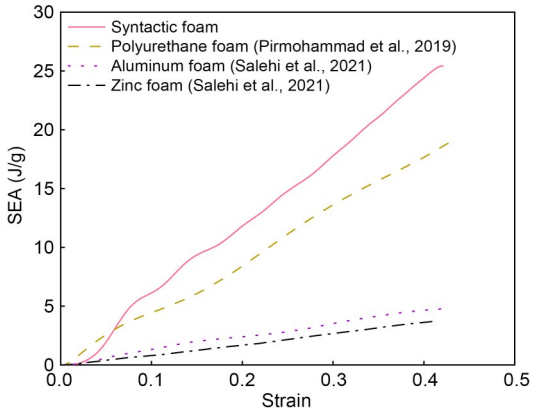

Fig. 19 SEA of different kinds of foam-filled tubes

(Pirmohammad et al., 2019), aluminum foam-filled tube (Salehi et al., 2021), and zinc foam-filled tube (Salehi et al., 2021). This is because the cenospheres in the syntactic foam can absorb more energy during the process of being crushed and compacted under impact load (Zhang et al., 2016). With the increase in impact velocity, the SEA of the specimen is slightly increased.

4 Comparative analysis of foam-filled tubes under different loading

To compare the deformation failure mode, mechanical characteristics, and energy absorption performance of foam-filled tubes under impact loading and quasi-static loading, specimen AX-T1.2-150 was selected for a quasi-static compression test. The quasi-static compression test was carried out on a universal testing machine with the loading speed of 1.8 mm/min.

4.1 Comparison of deformation modes

The deformation process of the specimen AX-T1.2-150 is presented in Fig. 20. The plastic deformation of the specimen is relatively concentrated, and only one fold is generated in the middle of the specimen under the impact loading. However, under quasi-static loading, three folds are uniformly formed along the height of the specimen, indicating that the plastic deformation of the specimen is greater. At the end of the quasi-static loading process, due to the asymmetric deformation of the specimen, the wall tube is partially torn. This is mainly due to machining errors and the inhomogeneity of materials, which lead to certain initial defects in the specimen. Compared with the impact

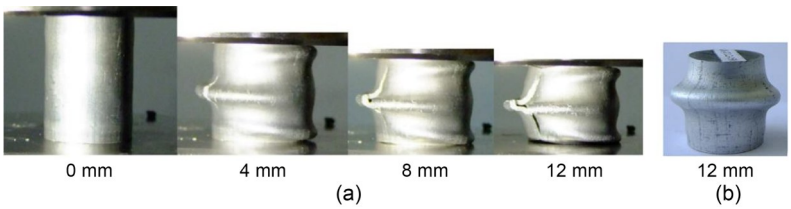

Fig. 20 Deformation mode of specimen AX-T1.2-150: (a) quasi-static loading; (b) impact loading

load, the loading rate of the quasi-static load is lower, which leads to more internal defect development of the material, and the tube wall cracks.

4.2 Comparison of mechanical characteristics and energy absorption performance

Fig. 21 shows the load–displacement curves of specimen AX-T1.2-150 under quasi-static loading and impact loading with impact velocity of 6 m/s. Table 3 is a comparison between the mechanical properties of specimen AX-T1.2-150 under two loading modes. As a result of the strain rate effect, the peak crushing load of the specimen under impact loading is 1.93 times of the quasi-static loading, and the mean crushing load also increases slightly.

To compare the energy absorption capacity of specimens under different loading modes more intuitively, the effective energy absorption ratio η is calculated as follows:

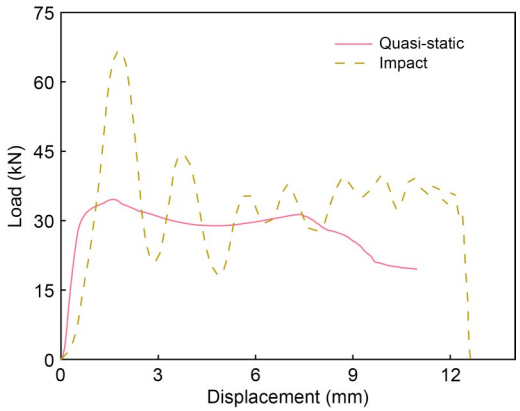

Fig. 21 Load–displacement curve of specimen AX-T1.2-150 under quasi-static loading and impact loading

Table 3 Mechanical properties of specimen AX-T1.2-150 under quasi-static loading and impact loading

Loading mode	Peak crushing load (kN)	Mean crushing load (kN)
Quasi-static loading	34.6	27.9
Impact loading	66.9	33.3

$$\eta = \frac{W_{\mathrm{ef}}}{W_{\mathrm{t}}}, \tag{7}$$

where W_{t} is the total energy applied by the test instrument during loading. The energy absorption capacity of specimen AX-T1.2-150 under two loading modes is shown in Fig. 22. It can be found that the effective energy absorption ratio of the syntactic foam-filled tube under impact loading is significantly higher than that under quasi-static loading, reaching 97.8%. Cenosphere-aluminum syntactic foam exhibits a higher stress level and energy absorption capacity under impact loading and is an excellent cushioning energy absorption material.

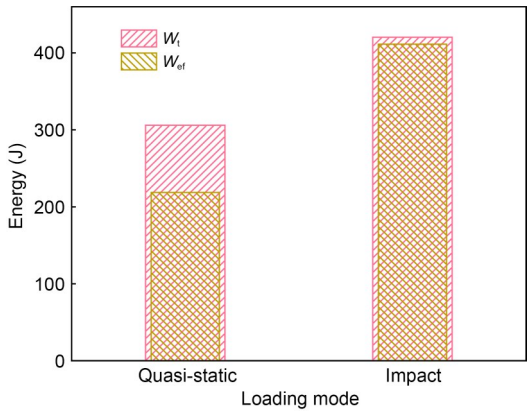

Fig. 22 Energy absorption capacity of specimen AX-T1.2-150 under quasi-static loading and impact loading

5 Conclusions

In this study, axial impact tests were carried out on different types of cenosphere-aluminum syntactic foam-filled tubes, and the failure mode of deformation, mechanical characteristics, and energy absorption performance of specimens under impact loading were studied. The influence of parameters such as pore size in syntactic foam and impact velocity was analyzed. On this basis, the crushing characteristics of foam-filled

tubes under different load conditions were compared and analyzed. The main findings include:

(1) Three kinds of syntactic foam-filled tubes buckled outwards in a concertina mode under impact loading, but the position and number of folds were different. With the increase of the pore size of syntactic foam filler, the plastic deformation capacity of the specimen increased.

(2) The aluminum tube can effectively limit the cracking of the filler, so that the initial peak crushing load and mean crushing load of the specimen were significantly improved. The increase in impact velocity had little effect on the mechanical properties of the specimen.

(3) The SEA of all cenosphere-aluminum syntactic foam-filled tubes under two impact velocities was higher than 15 J/g, and the SEA of 150SFFT reached 25 J/g, which is better than that of ordinary aluminum foam components.

(4) The peak load of 150SFFT under axial impact loading was 1.93 times that under quasi-static compression, and the mean crushing load increased slightly. The stress level of the material was increased under the impact loading, so the effective energy absorption ratio of the specimen reached 97.8%.

Acknowledgments

This work is supported by the National Natural Science Foundation of China (Nos. 51578201 and 51778196) and the Heilongjiang Provincial Natural Science Foundation of China (No. LH2020E058).

Author contributions

Boyi ZHANG and Wei WANG designed the research. Gaohui WU processed the corresponding data. Li WANG wrote the first draft of the manuscript. Jian ZHANG helped to organize the manuscript. Yuexin JIANG revised and edited the final version.

Conflict of interest

Li WANG, Boyi ZHANG, Jian ZHANG, Yuexin JIANG, Wei WANG, and Gaohui WU declare that they have no conflict of interest.

References

Abedi MM, Niknejad A, Liaghat GH, et al, 2018. Foam-filled grooved tubes with circular cross section under axial compression: an experimental study. *Iranian Journal of Science and Technology, Transactions of Mechanical Engineering*, 42(4):401-413. https://doi.org/10.1007/s40997-017-0106-0

Braszczyńska-Malik KN, Kamieniak J, 2017. AZ91 magnesium matrix foam composites with fly ash cenospheres fabricated by negative pressure infiltration technique. *Materials Characterization*, 128:209-216. https://doi.org/10.1016/j.matchar.2017.04.005

Djamaluddin F, Abdullah S, Ariffin AK, et al., 2015. Optimization of foam-filled double circular tubes under axial and oblique impact loading conditions. *Thin-Walled Structures*, 87:1-11. https://doi.org/10.1016/j.tws.2014.10.015

Doddamani M, Kishore, Shunmugasamy VC, et al., 2015. Compressive and flexural properties of functionally graded fly ash cenosphere–epoxy resin syntactic foams. *Polymer Composites*, 36(4):685-693. https://doi.org/10.1002/pc.22987

Duarte I, Krstulović-Opara L, Vesenjak M, 2018. Axial crush behaviour of the aluminium alloy in-situ foam filled tubes with very low wall thickness. *Composite Structures*, 192:184-192. https://doi.org/10.1016/j.compstruct.2018.02.094

Ferdynus M, Kotełko M, Urbaniak M, 2019. Crashworthiness performance of thin-walled prismatic tubes with corner dents under axial impact–numerical and experimental study. *Thin-Walled Structures*, 144:106239. https://doi.org/10.1016/j.tws.2019.106239

Garcia CD, Shahapurkar K, Doddamani M, et al., 2018. Effect of arctic environment on flexural behavior of fly ash cenosphere reinforced epoxy syntactic foams. *Composites Part B: Engineering*, 151:265-273. https://doi.org/10.1016/j.compositesb.2018.06.035

Ghahremanzadeh Z, Pirmohammad S, 2023. Crashworthiness performance of square, pentagonal, and hexagonal thin-walled structures with a new sectional design. *Mechanics of Advanced Materials and Structures*, 30(12):2353-2370. https://doi.org/10.1080/15376494.2022.2053910

Ghamarian A, Azarakhsh S, 2019. Axial crushing analysis of polyurethane foam-filled combined thin-walled structures: experimental and numerical analysis. *International Journal of Crashworthiness*, 24(6):632-644. https://doi.org/10.1080/13588265.2018.1506604

Guler MA, Cerit ME, Bayram B, et al., 2010. The effect of geometrical parameters on the energy absorption characteristics of thin-walled structures under axial impact loading. *International Journal of Crashworthiness*, 15(4):377-390. https://doi.org/10.1080/13588260903488750

Hanssen AG, Langseth M, Hopperstad OS, 2000. Static and dynamic crushing of circular aluminium extrusions with aluminium foam filler. *International Journal of Impact Engineering*, 24(5):475-507. https://doi.org/10.1016/S0734-743X(99)00170-0

Hou SJ, Li Q, Long SY, et al., 2007. Design optimization of regular hexagonal thin-walled columns with crashworthiness criteria. *Finite Elements in Analysis and Design*, 43(6-7):555-565. https://doi.org/10.1016/j.finel.2006.12.008

Hu DY, Wang YZ, Song B, et al., 2018. Energy absorption characteristics of a foam-filled tri-tube under axial quasi-static

loading: experiment and numerical simulation. *International Journal of Crashworthiness*, 23(4):417-432. https://doi.org/10.1080/13588265.2017.1331494

Hussein RD, Ruan D, Lu GX, et al., 2017. Crushing response of square aluminium tubes filled with polyurethane foam and aluminium honeycomb. *Thin-Walled Structures*, 110: 140-154. https://doi.org/10.1016/j.tws.2016.10.023

Kemény A, Movahedi N, Fiedler T, et al., 2022. The influence of infiltration casting technique on properties of metal syntactic foams and their foam-filled tube structures. *Materials Science and Engineering: A*, 852:143706. https://doi.org/10.1016/j.msea.2022.143706

Linul E, Movahedi N, Marsavina L, 2018. The temperature and anisotropy effect on compressive behavior of cylindrical closed-cell aluminum-alloy foams. *Journal of Alloys and Compounds*, 740:1172-1179. https://doi.org/10.1016/j.jallcom.2018.01.102

Liu Q, Fu J, Wang JS, et al., 2017. Axial and lateral crushing responses of aluminum honeycombs filled with EPP foam. *Composites Part B: Engineering*, 130:236-247. https://doi.org/10.1016/j.compositesb.2017.07.041

Liu ZF, Huang ZC, Qin QH, 2017. Experimental and theoretical investigations on lateral crushing of aluminum foam-filled circular tubes. *Composite Structures*, 175:19-27. https://doi.org/10.1016/j.compstruct.2017.05.004

Manakari V, Parande G, Gupta M, 2016. Effects of hollow fly-ash particles on the properties of magnesium matrix syntactic foams: a review. *Materials Performance and Characterization*, 5(1):116-131. https://doi.org/10.1520/MPC20150060

Mansor MA, Ahmad Z, Abdullah MR, 2022. Crashworthiness capability of thin-walled fibre metal laminate tubes under axial crushing. *Engineering Structures*, 252:113660. https://doi.org/10.1016/j.engstruct.2021.113660

Mohammadiha O, Ghariblu H, 2018. Crashworthiness study and optimisation of free inversion foam-filled tubes under dynamic loading. *International Journal of Crashworthiness*, 23(6):605-617. https://doi.org/10.1080/13588265.2017.1368119

Mondal DP, Das S, Ramakrishnan N, et al., 2009. Cenosphere filled aluminum syntactic foam made through stir-casting technique. *Composites Part A: Applied Science and Manufacturing*, 40(3):279-288. https://doi.org/10.1016/j.compositesa.2008.12.006

Movahedi N, Linul E, 2017. Quasi-static compressive behavior of the ex-situ aluminum-alloy foam-filled tubes under elevated temperature conditions. *Materials Letters*, 206: 182-184. https://doi.org/10.1016/j.matlet.2017.07.018

Movahedi N, Linul E, 2021. Radial crushing response of ex-situ foam-filled tubes at elevated temperatures. *Composite Structures*, 277:114634. https://doi.org/10.1016/j.compstruct.2021.114634

Movahedi N, Linul E, Marsavina L, 2018. The temperature effect on the compressive behavior of closed-cell aluminum-alloy foams. *Journal of Materials Engineering and Performance*, 27(1):99-108. https://doi.org/10.1007/s11665-017-3098-4

Movahedi N, Fiedler T, Taşdemirci A, et al., 2022. Impact loading of functionally graded metal syntactic foams. *Materials Science and Engineering: A*, 839:142831. https://doi.org/10.1016/j.msea.2022.142831

Pirmohammad S, Ahmadi-Saravani S, Zakavi SJ, 2019. Crashworthiness optimization design of foam-filled tapered decagonal structures subjected to axial and oblique impacts. *Journal of Central South University*, 26(10):2729-2745. https://doi.org/10.1007/s11771-019-4209-1

Sadighi A, Azimi MB, Asgari M, et al., 2022. Crashworthiness of hybrid composite-metal tubes with lateral corrugations in axial and oblique loadings. *International Journal of Crashworthiness*, 27(6):1813-1829. https://doi.org/10.1080/13588265.2021.2017654

Salehi M, Mirbagheri SMH, Ramiani AJ, 2021. Efficient energy absorption of functionally-graded metallic foam-filled tubes under impact loading. *Transactions of Nonferrous Metals Society of China*, 31(1):92-110. https://doi.org/10.1016/S1003-6326(20)65480-2

Sarkabiri B, Jahan A, Rezvani MJ, 2017. Crashworthiness multi-objective optimization of the thin-walled grooved conical tubes filled with polyurethane foam. *Journal of the Brazilian Society of Mechanical Sciences and Engineering*, 39(7):2721-2734. https://doi.org/10.1007/s40430-017-0747-3

Su MM, Wang H, Hao H, 2019. Axial and radial compressive properties of alumina-aluminum matrix syntactic foam filled thin-walled tubes. *Composite Structures*, 226:111197. https://doi.org/10.1016/j.compstruct.2019.111197

Sun GY, Li GY, Hou SJ, et al., 2010. Crashworthiness design for functionally graded foam-filled thin-walled structures. *Materials Science and Engineering: A*, 527(7-8):1911-1919. https://doi.org/10.1016/j.msea.2009.11.022

Sun GY, Li SF, Liu Q, et al., 2016. Experimental study on crashworthiness of empty/aluminum foam/honeycomb-filled CFRP tubes. *Composite Structures*, 152:969-993. https://doi.org/10.1016/j.compstruct.2016.06.019

Sun GY, Li SF, Li GY, et al., 2018. On crashing behaviors of aluminium/CFRP tubes subjected to axial and oblique loading: an experimental study. *Composites Part B: Engineering*, 145:47-56. https://doi.org/10.1016/j.compositesb.2018.02.001

Wang L, Zhang BY, Zhang J, et al., 2021. Deformation and energy absorption properties of cenosphere-aluminum syntactic foam-filled tubes under axial compression. *Thin-Walled Structures*, 160:107364. https://doi.org/10.1016/j.tws.2020.107364

Wang Z, Jin XH, Li Q, et al., 2019. On crashworthiness design of hybrid metal-composite structures. *International Journal of Mechanical Sciences*, 171:105380. https://doi.org/10.1016/j.ijmecsci.2019.105380

Wu SY, Li GY, Sun GY, et al., 2016. Crashworthiness analysis and optimization of sinusoidal corrugation tube. *Thin-Walled Structures*, 105:121-134. https://doi.org/10.1016/j.tws.2016.03.029

Xu BY, Sun GY, Wu S, et al., 2017. Crashworthiness analysis and optimization of Fourier varying section tubes. *International Journal of Non-Linear Mechanics*, 92:41-58. https://doi.org/10.1016/j.ijnonlinmec.2017.03.001

Yan LB, Chouw N, Jayaraman K, 2014. Lateral crushing of empty and polyurethane-foam filled natural flax fabric reinforced epoxy composite tubes. *Composites Part B: Engineering*, 63:15-26. https://doi.org/10.1016/j.compositesb.2014.03.013

Zha YB, Wang S, Ma QH, et al., 2022. Study on the axial impact of Al-CFRP thin-walled tubes with induced design. *Polymer Composites*, 43(7):4660-4686. https://doi.org/10.1002/pc.26720

Zhang BY, Lin YF, Li S, et al., 2016. Quasi-static and high strain rates compressive behavior of aluminum matrix syntactic foams. *Composites Part B: Engineering*, 98:288-296. https://doi.org/10.1016/j.compositesb.2016.05.034

Zhang BY, Zhang J, Wang L, et al., 2021. Bending behavior of cenosphere aluminum matrix syntactic foam-filled circular tubes. *Engineering Structures*, 243:112650. https://doi.org/10.1016/j.engstruct.2021.112650

Zhang ZY, Sun W, Zhao YS, et al., 2018. Crashworthiness of different composite tubes by experiments and simulations. *Composites Part B: Engineering*, 143:86-95. https://doi.org/10.1016/j.compositesb.2018.01.021

Zou X, Gao GJ, Dong HP, et al., 2017. Crashworthiness analysis and structural optimisation of multi-cell square tubes under axial and oblique loads. *International Journal of Crashworthiness*, 22(2):129-147. https://doi.org/10.1080/13588265.2016.1235109